

Dose Deposits from ^{90}Y , ^{177}Lu , ^{111}In , and ^{161}Tb in Micrometastases of Various Sizes: Implications for Radiopharmaceutical Therapy

**Elif Hindié¹, Paolo Zanotti-Fregonara¹, Michele A. Quinto², Clément Morgat¹,
Christophe Champion²**

*¹CHU de Bordeaux, Service de Médecine Nucléaire, CNRS-UMR 5287, LabEx TRAIL,
Université de Bordeaux, France.*

*²Université de Bordeaux, CNRS/IN2P3, Centre d'Etudes Nucléaires de Bordeaux
Gradignan (CENBG), France*

Corresponding authors:

- Pr Elif Hindié, MD, PhD

Service de Médecine Nucléaire, Hôpital Haut-Lévêque,

CHU de Bordeaux, 33604 Pessac, France.

Tel: +(33)557656838; Fax: +(33)557656839

e-mail: elif.hindie@chu-bordeaux.fr

- Pr Christophe Champion

e-mail: champion@cenbg.in2p3.fr

Financial support: This work was funded by the Institut National de la Santé et de la Recherche Médicale (INSERM) under contract PhysiCancer “MICRONAUTE project” and by the French Investment for the Future program within LabEx TRAIL ANR-10-LABX-57

Total word count: 4996

Running foot line: Dose deposits in micrometastases

ABSTRACT

Radiopharmaceutical therapy, traditionally limited to refractory metastatic cancer, is being increasingly used at earlier stages, such as for treating minimal residual disease. The aim of this study was to compare the effectiveness of yttrium-90, lutetium-177, indium-111 and terbium-161 at irradiating “micrometastases”. ^{90}Y and ^{177}Lu are widely used β^- emitting radionuclides. ^{161}Tb is a medium-energy β^- isotope, which is similar to ^{177}Lu but emits a higher percentage of conversion and Auger electrons. ^{111}In emits γ photons, conversion and Auger electrons.

METHODS: We used the Monte Carlo code CELLDOSE to assess electron doses from a uniform distribution of ^{90}Y , ^{177}Lu , ^{111}In or ^{161}Tb in spheres with diameters ranging from 10mm to 10 μm . Because these isotopes differ in electron energy per decay, the doses were compared assuming that 1 MeV was released per μm^3 , which would result in 160Gy if totally absorbed.

RESULTS: In a 10-mm sphere, the doses delivered by ^{90}Y , ^{177}Lu , ^{111}In and ^{161}Tb were 96.5Gy, 152Gy, 153Gy and 152Gy, respectively. The doses decreased along with the decrease in sphere size, and more abruptly so for ^{90}Y . In a 100- μm metastasis, the dose delivered by ^{90}Y was only 1.36Gy, compared to 24.5Gy for ^{177}Lu , 38.9Gy for ^{111}In and 44.5Gy for ^{161}Tb . In cell-sized spheres, the dose delivered by ^{111}In and ^{161}Tb was higher than that of ^{177}Lu . For instance, in a 10- μm cell, ^{177}Lu delivered 3.92Gy, compared to 22.8Gy for ^{111}In and 14.1Gy for ^{161}Tb .

CONCLUSION: ^{177}Lu , ^{111}In and ^{161}Tb might be more appropriate than ^{90}Y for treating minimal residual disease. Terbium-161 is a promising isotope because it combines the advantages of a medium-energy β^- emission with those of Auger electrons, and emits fewer photons than ^{111}In .

Key words: Radiopharmaceutical therapy, ^{90}Y , ^{177}Lu , ^{111}In , ^{161}Tb

INTRODUCTION

The main advantage of radiopharmaceutical therapy over conventional external beam radiotherapy is the ability to reach metastases and tumor cells scattered in multiple body locations (1). It uses tumor-targeting radiopharmaceuticals, such as ^{131}I -MIBG for neural crest-derived tumors, ^{131}I - or ^{90}Y -labelled anti-CD20 antibodies for lymphoma, the somatostatin analogs ^{90}Y -DOTATOC and ^{177}Lu -DOTATATE for neuroendocrine tumors, or PSMA-targeting molecules for prostate cancer (2-5).

Radiopharmaceutical therapy is not limited anymore to “palliative” care in patients with relapsed/refractory disease, but now includes early treatment of metastatic disease, adjuvant therapy, and consolidation after remission, as for example in non-Hodgkin lymphomas (6,7). Indeed, adjuvant iodine-131 therapy is known to prevent recurrence after thyroidectomy (8). Also, radiopharmaceutical therapy achieves better results when the metastases are small (4,9). Large metastases are difficult to irradiate effectively because they often include areas of stromal, fibrous, or necrotic tissues, as well as tumor areas with loss of target expression. Moreover, hypoxia increases resistance to radiation. Experimental data in rodents also showed better efficacy on microscopic metastases (10,11).

In many cancers, prognosis is linked to metastatic relapse which may occur years after primary surgery (12). Relapse can be predicted from various parameters, including the initial locoregional extension, tumor grade, response to neoadjuvant treatment, and tumor markers levels. Moreover, metastatic spread can now be diagnosed at a very early stage, for example by detecting tumor cells in the bone marrow or blood (13,14). Therefore, radiopharmaceutical therapy may play an important role to eradicate occult micrometastases in high-risk patients.

It is, however, unclear which isotopes would be the most appropriate for adjuvant or consolidation therapy, where tumor targets are undetectable by radiological examinations and presumably very small (ranging from isolated tumor cells to lesions of 5-10 mm of diameter). Although ^{90}Y showed encouraging results for treating occult residual disease

after remission of ovarian cancer (15) and lymphoma (6,7), isotopes with lower energy might be a better choice.

^{90}Y (high-energy β^-) and ^{177}Lu (medium-energy β^-) are the two most widely used isotopes for labeling therapeutic radiopharmaceuticals (2-5). Indium-111 is a γ -emitting isotope mainly used for imaging. However, it also emits Auger and conversion electrons (CE) and might be used to target micrometastases and single cells (16-18). The radiolanthanide terbium-161 is a medium-energy β^- emitter similar to ^{177}Lu but emits a higher percentage of conversion and Auger electrons. Some in vivo studies suggested that ^{161}Tb might outperform ^{177}Lu (19,20). The aim of this Monte Carlo simulation study was to compare the effectiveness of ^{90}Y , ^{177}Lu , ^{111}In and ^{161}Tb at irradiating micrometastases of various sizes.

MATERIAL AND METHODS

The Monte Carlo code “CELLDOSE” was used to assess electron dose from a uniform distribution of ^{90}Y , ^{177}Lu , ^{111}In or ^{161}Tb in spheres of water density whose diameters ranged from 10mm to 10 μm . The decay characteristics of these isotopes are shown in Table-1. The full data on electron emissions (β -spectra, CE, Auger and Coster-Kronig electrons) were obtained from the International Commission on Radiological Protection (ICRP) publication: ICRP-07 (21). The electron emission spectra used in the Monte Carlo simulation are shown in Figure-1. Photons were neglected.

CELLDOSE is based on electron-water molecule interaction cross sections and takes into account all ionizations, excitations and elastic scatterings in order to produce an event-by-event electron track simulation (22). The full slowing-down histories for primary and secondary electrons are described until an energy value of 7.4 eV is reached (electronic excitation threshold of the water molecule) (23). The residual energy below this cut-off was

considered to be absorbed locally. Figure-2 shows the energy deposits along the paths of two conversion electrons (one from ^{111}In and one from ^{161}Tb), and two Auger electrons.

For each isotope and sphere we assessed the absorbed energy as well as the relative contribution of β^- particles, CE and Auger electrons (as we previously described for iodine-131 (22)).

In addition to the dose resulting from a single decay (S-values), we also calculated in all spheres the absorbed dose resulting from a uniform concentration (1 decay per μm^3). Moreover, because the four isotopes have a different electron energy emitted per decay, absorbed doses were compared after normalizing by a fixed amount of electron energy released per unit of volume (1 MeV per μm^3). This concentration would yield 160Gy if totally absorbed.

Finally, to assess the ability of each isotope to deliver a cross-dose outside labeled structures, we studied the spatial profile of energy deposit around a point source.

RESULTS

Absorbed Energy and Contribution of the Different Electron Emissions

For each isotope, Table-2 reports the energy absorbed in each sphere and the relative contribution of the various electron emissions. The absorbed energy decreases along with the decrease in sphere size. This decrease was more pronounced in the case of ^{90}Y (Table 2).

For ^{177}Lu , the combined contribution of CE and Auger electrons to absorbed energy was 10% in the 10-mm sphere and reached 33.9% in the 10- μm sphere (Table 2). The contribution of CE and Auger electrons was much higher in the case of ^{161}Tb and was 24.9% of the energy deposit in the 10-mm sphere and 88.3% in the 10- μm sphere (Table 2). Considering ^{111}In , the relative contribution of Auger electrons increased compared to that of CE when the sphere size decreased.

S Values for ⁹⁰Y, ¹⁷⁷Lu, ¹¹¹In, and ¹⁶¹Tb in Spheres of Various Sizes

S-values obtained with the Monte Carlo code CELLDOSE are reported in Table-3. There was good agreement with S-values previously reported for ⁹⁰Y and ¹⁷⁷Lu using scaled dose point kernel (24) and for ⁹⁰Y and ¹¹¹In using range-energy expressions for electrons (25). The largest differences were found for ⁹⁰Y in the 5000- μ m sphere: The S-value reported by Goddu was 11% lower, while that reported by Bardiès was 5.4% higher, than the value obtained with CELLDOSE (24,25). Terbium-161 data were not available in the literature for comparison.

Absorbed Doses from ⁹⁰Y, ¹⁷⁷Lu, ¹¹¹In, and ¹⁶¹Tb after Normalization

Table-3 and Figure-3 show, for each isotope and sphere, the absorbed dose from 1 decay per μm^3 and the absorbed dose from 1 MeV released per μm^3 (i.e. normalization for differences in electron energy per decay). Please note that based on the total electron energy per decay (Table 1), the average number of decays per cubic micrometer (N) that corresponds to 1 MeV released per cubic micrometer is: 1.07 for ⁹⁰Y, 6.76 for ¹⁷⁷Lu, 28.74 for ¹¹¹In or 4.94 for ¹⁶¹Tb. Also, assuming complete decay and no biological excretion and/or redistribution over time, and a tissue density of $1\text{g}/\text{cm}^3$, this corresponds to an activity concentration within tumor tissue ($A_0 = N \times \ln 2 / T$) of: 3.22 MBq/g for ⁹⁰Y, 8.16 MBq/g for ¹⁷⁷Lu, 82.19 MBq/g for ¹¹¹In or 5.74 MBq/g for ¹⁶¹Tb.

When 1 MeV was released in every μm^3 , the absorbed dose for a 10-mm metastasis was 96.5Gy with ⁹⁰Y, 152Gy with ¹⁷⁷Lu, 153Gy with ¹¹¹In and 152Gy with ¹⁶¹Tb (Table 3). However, in a 1-mm metastasis, the dose delivered by ⁹⁰Y fell to 13.3Gy as compared to 104Gy with ¹⁷⁷Lu, 118Gy with ¹¹¹In and 108Gy with ¹⁶¹Tb. For a 100- μ m micrometastasis, the absorbed dose was only 1.36Gy with ⁹⁰Y, but 24.5Gy with ¹⁷⁷Lu, 38.9Gy with ¹¹¹In and 44.5Gy with ¹⁶¹Tb (Table 3 and Fig. 3).

In cell-sized spheres, ¹¹¹In and ¹⁶¹Tb delivered significantly higher doses than ¹⁷⁷Lu. For instance, in a homogeneously labeled single cell of 10 μ m diameter, the absorbed dose was 3.92Gy for ¹⁷⁷Lu, 22.8Gy for ¹¹¹In and 14.1Gy for ¹⁶¹Tb (Table 3 and Fig. 3).

Energy Deposit around a Point Source

Figure-4 shows the pattern of energy deposit after normalization (1 MeV released). The radius within which 90% of the energy is deposited (R90) is 5.82 mm for ^{90}Y , 0.62 mm for ^{177}Lu , 0.37 mm for ^{111}In , and 0.63mm for ^{161}Tb . The radius within which 99% of the energy is deposited (R99) is 8.19 mm for ^{90}Y , 1.07 mm for ^{177}Lu , 0.49 mm for ^{111}In , and 1.06 mm for ^{161}Tb . At a distance beyond 0.8 mm, ^{90}Y deposited more energy (per MeV released) than ^{177}Lu or ^{161}Tb .

The complex profile of energy deposit from ^{111}In shows a high peak, four times higher than that of ^{177}Lu (per MeV released), in the first 10- μm thick shell surrounding the point source (Fig. 4C).

The pattern of energy deposit of ^{161}Tb and ^{177}Lu markedly differed in proximity of the source. The energy deposited by ^{161}Tb (per MeV released) was higher than that deposited by ^{177}Lu up to 30 μm around the point source, and particularly so in the first 10 μm (Fig. 4D).

DISCUSSION

The majority of currently used radiopharmaceuticals were designed to be administered to patients with advanced disease and the choice of the radionuclide had been made accordingly. However, the same radiopharmaceuticals might not be equally effective to treat both large tumor masses and minimal residual disease. For example, anti-CD20 antibodies, labeled with ^{90}Y , have been used to treat patients with relapsed/refractory lymphomas (2), but are now also used for consolidation after successful chemotherapy (6,7). In radionuclide therapy, there is an “optimal tumor size for cure” which differs from one radionuclide to another (26,27). Thanks to the high energy of ^{90}Y β^- particles, ^{90}Y -labeled radiopharmaceuticals may compensate for uptake heterogeneity within large tumors and effectively irradiate non-labeled targets, such as liver malignancies after intra-arterial radioembolization (28). At a distance beyond 0.8mm, ^{90}Y deposited more energy (per MeV released) than ^{177}Lu (Fig. 4). However, our results clearly suggest that ^{90}Y is not an

adequate isotope for eradicating micrometastases, because most of the energy was deposited outside the tumor (Table 2). This is expected to reduce efficacy and increase toxicity. Lutetium-177 irradiated smaller spheres more effectively than ^{90}Y .

To facilitate the comparison between isotopes, the energy released was normalized for 1 MeV per μm^3 of tumor tissue. If totally absorbed, this energy would yield 160 Gy. The normalized dose in a 1-cm metastasis was 96Gy with ^{90}Y (vs. 152Gy with ^{177}Lu). However, the dose delivered by ^{90}Y steeply decreased when sphere size decreased (Table 3 and Fig. 3B). In a 1-mm metastasis, the dose from ^{90}Y was 13.3Gy (vs. 104Gy with ^{177}Lu). In a 100- μm micrometastasis, the dose from ^{90}Y was only 1.36Gy, while ^{177}Lu delivered 24.5Gy.

These results are in line with experimental data by Michel and colleagues, who showed that the rate of eradication of single cells and micrometastases was higher with ^{177}Lu than with ^{90}Y (29). By contrast, one study assessed anti-CD20 pretargeted radioimmunotherapy on lymphoma xenografts and found a higher efficacy with ^{90}Y (30). However, the treatment was given when the size of tumor xenografts exceeded 8 mm (which is higher than the size of a typical micrometastasis). Radioactivity distribution within the tumor was highly heterogeneous (30). Also, because tumor uptake (I.D./g) decreased over time (11.8% at 4h; 3.7% at 120h), the longer half-life of ^{177}Lu was here a drawback. Finally, ^{90}Y and ^{177}Lu were compared using the same activity (37MBq), although the amount of energy released differs.

Although ^{177}Lu performed better than ^{90}Y in small metastases, ^{111}In and ^{161}Tb outperformed ^{177}Lu in very small metastases (<100 μm) and single cells (Table 3 and Fig. 3B).

The dose delivered by ^{111}In (considering 1 MeV released per μm^3) was 1.6 times higher than that from ^{177}Lu in a 100- μm micrometastasis (38.9Gy vs. 24.5Gy) and 5.8 times higher than that from ^{177}Lu in a 10- μm cell (22.8Gy vs. 3.92Gy) (Table 3). Studies have shown that the rate of eradication of micrometastases and single cells is higher with ^{111}In

than with either ^{90}Y (16) or ^{177}Lu (29). By consequence, many teams actively work on developing ^{111}In -labeled radiopharmaceuticals aimed at targeting micrometastases or cancer stem cells (17,18). ^{111}In has, however, a large proportion of photon emission (92% of the total energy per decay) (Table 1). Photon emission adds to the total body dose and in many countries requires patient hospitalization for radiation protection purposes. The alternatives offered by ^{161}Tb are then of major interest.

Terbium-161 has a β^- spectrum similar to that of ^{177}Lu , but emits a larger number of Auger and CE (Fig. 1). Most ^{161}Tb CE are in the low energy domain (<50keV) and deposit their dose over relatively short distances (Figs. 1 and 2). The dose delivered by ^{161}Tb (considering 1 MeV released per μm^3) is 1.8 times higher than that delivered by ^{177}Lu in a 100- μm micrometastasis (44.5Gy vs. 24.5Gy) and 3.6 times higher than ^{177}Lu in a 10- μm cell (14.1Gy vs. 3.9Gy) (Table 3). ^{161}Tb deposits a larger amount of energy per MeV than ^{177}Lu over a distance of 30 μm (Fig. 4D). Thus, ^{161}Tb would likely deliver a higher dose than ^{177}Lu , not only to the targeted cell, but also to its immediate neighbors.

Our Monte Carlo simulation provides a mechanistic rationale to the studies that found a good tumor-control efficacy of ^{161}Tb -labeled molecules. For example, ^{161}Tb -anti-L1CAM antibodies were more effective than ^{177}Lu -anti-L1CAM at inhibiting the growth of subcutaneous xenografts of ovarian cancer (19). In another study, the radioactivity concentration necessary to achieve half-maximal inhibition of tumor cells was lower with ^{161}Tb -labeled than with ^{177}Lu -labeled radiofolate conjugates (20).

The most suitable radioisotope can be appropriately chosen if the subcellular distribution of the targeting molecule is known. Techniques such as high-resolution autoradiography or secondary ion mass spectrometry can quantitatively depict the distribution at the cellular level (31). This distribution may be used as input to derive the absorbed dose with Monte Carlo codes (32,33). Uniform distribution, as considered in the present study, is an acceptable model for some molecules which are internalized via receptor-mediated endocytosis and partly trafficked to the nucleus. Examples include growth factors such as EGF, or agonist analogs of somatostatin and bombesin (4,17,34). By

contrast, neuropeptide antagonists are not internalized (34). Again, some antibodies are internalized after binding to their membrane receptor (e.g. antibodies targeting CD22, PSMA, EGFR, HER2), whereas others (e.g. anti-CD20 and anti-CEA) are less internalized. Many research projects aim at facilitating the routing of Auger emitting radiopharmaceuticals to the nucleus (18,35). For DNA irradiation, internalization in the nucleus is indeed necessary to get the full benefit from Auger electrons (Fig. 2B). Auger electrons may also effectively irradiate other targets, such as cell membranes (36).

Our study may help predicting the effectiveness of adjuvant therapy in clinical trials. We ran our simulation by assuming that 1 MeV was released per μm^3 . If totally absorbed, this energy would yield 160Gy using any isotope. Notably, this value is within the range of tumor-absorbed doses that were measured in metastases of neuroendocrine tumors in patients who showed good response to ^{177}Lu -DOTATATE therapy (37). If the same activity of ^{177}Lu -DOTATATE that is used for treating radiological metastases was given as adjuvant therapy, and assuming that the uptake in occult metastases is the same (1 MeV released per μm^3), the radiation dose would decrease along with the size of targeted metastases. The predicted dose would be 104Gy in a 1-mm metastasis, 24.5Gy in a 100- μm micrometastasis, and 3.9Gy in a 10- μm single tumor cell. Although small tumors are more radiosensitive than macrometastases (10,11), the low dose delivered by ^{177}Lu to isolated cells might not be sufficient to destroy them all. However, the dose delivered by a hypothetical ^{161}Tb -labeled somatostatin analogue (with the same tumor affinity) would be 1.8 times higher in a 100- μm micrometastasis (44.5Gy) and 3.6 times higher in a 10- μm single cell (14.1Gy) (Table 3).

Similarly to ^{177}Lu , ^{161}Tb can be stably linked to various targeting molecules (19,20). It has a small percentage of photons that would enable post-therapy imaging (Table 1). Moreover, two isotopes of terbium (^{152}Tb ; $T_{1/2} = 17.5\text{h}$; β^+ emitter and ^{155}Tb ; $T_{1/2} = 5.32\text{d}$; γ -emitter) offer the possibility for pre-therapy imaging and dosimetry with PET or SPECT.

^{161}Tb can be produced as no carrier added in large amounts, using for example a gadolinium-160 target ($^{160}\text{Gd}(n,\gamma)^{161}\text{Tb}$), and with good radionuclide purity (^{160}Tb to ^{161}Tb

activity ratio <0.0001) (38). The cost for large-scale production was estimated to be comparable to that of no carrier added ^{177}Lu (38).

CONCLUSION

Radiopharmaceutical therapy can effectively target disseminated tumor cells and occult micrometastases, provided that the optimal isotope is used. ^{177}Lu , ^{111}In and ^{161}Tb might be more appropriate than ^{90}Y for treating minimal residual disease. Terbium-161 combines the classical advantages of a medium-energy β^- isotope and those specific to Auger emitters. In addition, ^{161}Tb emits fewer photons than ^{111}In . These promising characteristics warrant the use of ^{161}Tb in clinical trials.

ACKNOWLEDGMENTS

We thank Pr. Keith Eckerman for helpful discussions regarding the ICRP-107 data files.

References

1. Volkert WA, Hoffman TJ. Therapeutic radiopharmaceuticals. *Chem Rev.* 1999;99:2269-2292.
2. Witzig TE, Gordon LI, Cabanillas F, et al. Randomized controlled trial of yttrium-90-labeled ibritumomab tiuxetan radioimmunotherapy versus rituximab immunotherapy for patients with relapsed or refractory low-grade, follicular, or transformed B-cell non-Hodgkin's lymphoma. *J Clin Oncol.* 2002;20:2453-2463.
3. Waldherr C, Pless M, Maecke HR, et al. Tumor response and clinical benefit in neuroendocrine tumors after 7.4 GBq (90)Y-DOTATOC. *J Nucl Med.* 2002;43:610-616.
4. Kwekkeboom DJ, de Herder WW, Kam BL, et al. Treatment with the radiolabeled somatostatin analog [177 Lu-DOTA 0,Tyr3]octreotate: toxicity, efficacy, and survival. *J Clin Oncol.* 2008;26:2124-2130.
5. Kratochwil C, Giesel FL, Eder M, et al. [¹⁷⁷Lu]Lutetium-labelled PSMA ligand-induced remission in a patient with metastatic prostate cancer. *Eur J Nucl Med Mol Imaging.* 2015;42:987-988.
6. Morschhauser F, Radford J, Van Hoof A, et al. Phase III trial of consolidation therapy with yttrium-90-ibritumomab tiuxetan compared with no additional therapy after first remission in advanced follicular lymphoma. *J Clin Oncol.* 2008;26:5156-5164.
7. Witzig TE, Hong F, Micallef IN, et al. A phase II trial of RCHOP followed by radioimmunotherapy for early stage (stages I/II) diffuse large B-cell non-Hodgkin lymphoma: ECOG3402. *Br J Haematol.* 2015;170:679-686.

8. Mazzaferri EL, Jhiang SM. Long-term impact of initial surgical and medical therapy on papillary and follicular thyroid cancer. *Am J Med.* 1994;97:418-428.
9. Hindié E, Zanotti-Fregonara P, Keller I, et al. Bone metastases of differentiated thyroid cancer: impact of early 131I-based detection on outcome. *Endocr Relat Cancer.* 2007;14:799-807.
10. Aarts F, Koppe MJ, Hendriks T, et al. Timing of adjuvant radioimmunotherapy after cytoreductive surgery in experimental peritoneal carcinomatosis of colorectal origin. *Ann Surg Oncol.* 2007;14:533-540.
11. de Jong GM, Hendriks T, Eek A, et al. Radioimmunotherapy improves survival of rats with microscopic liver metastases of colorectal origin. *Ann Surg Oncol.* 2009;16:2065-2073.
12. Pantel K, Alix-Panabières C, Riethdorf S. Cancer micrometastases. *Nat Rev Clin Oncol.* 2009;6:339-351.
13. Braun S, Pantel K, Müller P, et al. Cytokeratin-positive cells in the bone marrow and survival of patients with stage I, II, or III breast cancer. *N Engl J Med.* 2000;342:525-533.
14. Bork U, Rahbari NN, Schölch S, et al. Circulating tumour cells and outcome in non-metastatic colorectal cancer: a prospective study. *Br J Cancer.* 2015;112:1306-1313.
15. Oei AL, Verheijen RH, Seiden MV, et al. Decreased intraperitoneal disease recurrence in epithelial ovarian cancer patients receiving intraperitoneal consolidation treatment with yttrium-90-labeled murine HMFG1 without improvement in overall survival. *Int J Cancer.* 2007;120:2710-2714.

16. Ochakovskaya R, Osorio L, Goldenberg DM, Mattes MJ. Therapy of disseminated B-cell lymphoma xenografts in severe combined immunodeficient mice with an anti-CD74 antibody conjugated with (111)indium, (67)gallium, or (90)yttrium. *Clin Cancer Res.* 2001;7:1505-1510.
17. Vallis KA, Reilly RM, Scollard D, et al. Phase I trial to evaluate the tumor and normal tissue uptake, radiation dosimetry and safety of (111)In-DTPA-human epidermal growth factor in patients with metastatic EGFR-positive breast cancer. *Am J Nucl Med Mol Imaging.* 2014;4:181-192.
18. Leyton JV, Gao C, Williams B, Keating A, Minden M, Reilly RM. A radiolabeled antibody targeting CD123(+) leukemia stem cells - initial radioimmunotherapy studies in NOD/SCID mice engrafted with primary human AML. *Leuk Res Rep.* 2015;4:55-59.
19. Grünberg J, Lindenblatt D, Dorrer H, et al. Anti-L1CAM radioimmunotherapy is more effective with the radiolanthanide terbium-161 compared to lutetium-177 in an ovarian cancer model. *Eur J Nucl Med Mol Imaging.* 2014;41:1907-1915.
20. Müller C, Reber J, Haller S, et al. Direct in vitro and in vivo comparison of (161)Tb and (177)Lu using a tumour-targeting folate conjugate. *Eur J Nucl Med Mol Imaging.* 2014;41:476-485.
21. Eckerman K, Endo A. ICRP Publication 107. Nuclear decay data for dosimetric calculations. *Ann ICRP* 2008;38:7-96.
22. Champion C, Zanotti-Fregonara P, Hindié E. CELLDOSE: a Monte Carlo code to assess electron dose distribution--S values for 131I in spheres of various sizes. *J Nucl Med.* 2008;49:151-157.

23. Champion C. Theoretical cross sections for electron collisions in water: structure of electron tracks. *Phys Med Biol.* 2003;48:2147-2168.
24. Bardiès M, Chatal JF. Absorbed doses for internal radiotherapy from 22 beta-emitting radionuclides: beta dosimetry of small spheres. *Phys Med Biol.* 1994;39:961-981.
25. Goddu SM, Rao DV, Howell RW. Multicellular dosimetry for micrometastases: dependence of self-dose versus cross-dose to cell nuclei on type and energy of radiation and subcellular distribution of radionuclides. *J Nucl Med.* 1994;35:521-530.
26. O'Donoghue JA, Bardiès M, Wheldon TE. Relationships between tumor size and curability for uniformly targeted therapy with beta-emitting radionuclides. *J Nucl Med.* 1995;36:1902-1909.
27. Bernhardt P, Forssell-Aronsson E, Jacobsson L, Skarnemark G. Low-energy electron emitters for targeted radiotherapy of small tumours. *Acta Oncol.* 2001;40:602-608.
28. Mazzaferro V, Sposito C, Bhoori S, et al. Yttrium-90 radioembolization for intermediate-advanced hepatocellular carcinoma: a phase 2 study. *Hepatology.* 2013;57:1826-1837.
29. Michel RB, Andrews PM, Rosario AV, Goldenberg DM, Mattes MJ. ¹⁷⁷Lu-antibody conjugates for single-cell kill of B-lymphoma cells in vitro and for therapy of micrometastases in vivo. *Nucl Med Biol.* 2005;32:269-278.
30. Frost SH, Frayo SL, Miller BW, et al. Comparative efficacy of ¹⁷⁷Lu and ⁹⁰Y for anti-CD20 pretargeted radioimmunotherapy in murine lymphoma xenograft models. *PLoS One.* 2015;10:e0120561.

31. Chéhadé F, de Labriolle-Vaylet C, Moins N, et al. Secondary ion mass spectrometry as a tool for investigating radiopharmaceutical distribution at the cellular level: the example of I-BZA and (14)C-I-BZA. *J Nucl Med.* 2005;46:1701-1706.
32. Hindié E, Champion C, Zanotti-Fregonara P, et al. Calculation of electron dose to target cells in a complex environment by Monte Carlo code "CELLDOSE". *Eur J Nucl Med Mol Imaging.* 2009;36:130-136.
33. Falzone N, Fernández-Varea JM, Flux G, Vallis KA. Monte Carlo evaluation of Auger electron-emitting theragnostic radionuclides. *J Nucl Med.* 2015;56:1441-1446.
34. Morgat C, Mishra AK, Varshney R, Allard M, Fernandez P, Hindié E. Targeting neuropeptide receptors for cancer imaging and therapy: perspectives with bombesin, neurotensin, and neuropeptide-Y receptors. *J Nucl Med.* 2014;55:1650-1657.
35. Kassis AI. The amazing world of auger electrons. *Int J Radiat Biol.* 2004;80:789-803.
36. Pouget JP, Santoro L, Raymond L, et al. Cell membrane is a more sensitive target than cytoplasm to dense ionization produced by auger electrons. *Radiat Res.* 2008;170:192-200.
37. Ilan E, Sandström M, Wassberg C, et al. Dose response of pancreatic neuroendocrine tumors treated with peptide receptor radionuclide therapy using 177Lu-DOTATATE. *J Nucl Med.* 2015;56:177-182.
38. Lehenberger S, Barkhausen C, Cohrs S, et al. The low-energy $\beta(-)$ and electron emitter (161)Tb as an alternative to (177)Lu for targeted radionuclide therapy. *Nucl Med Biol.* 2011;38:917-924.

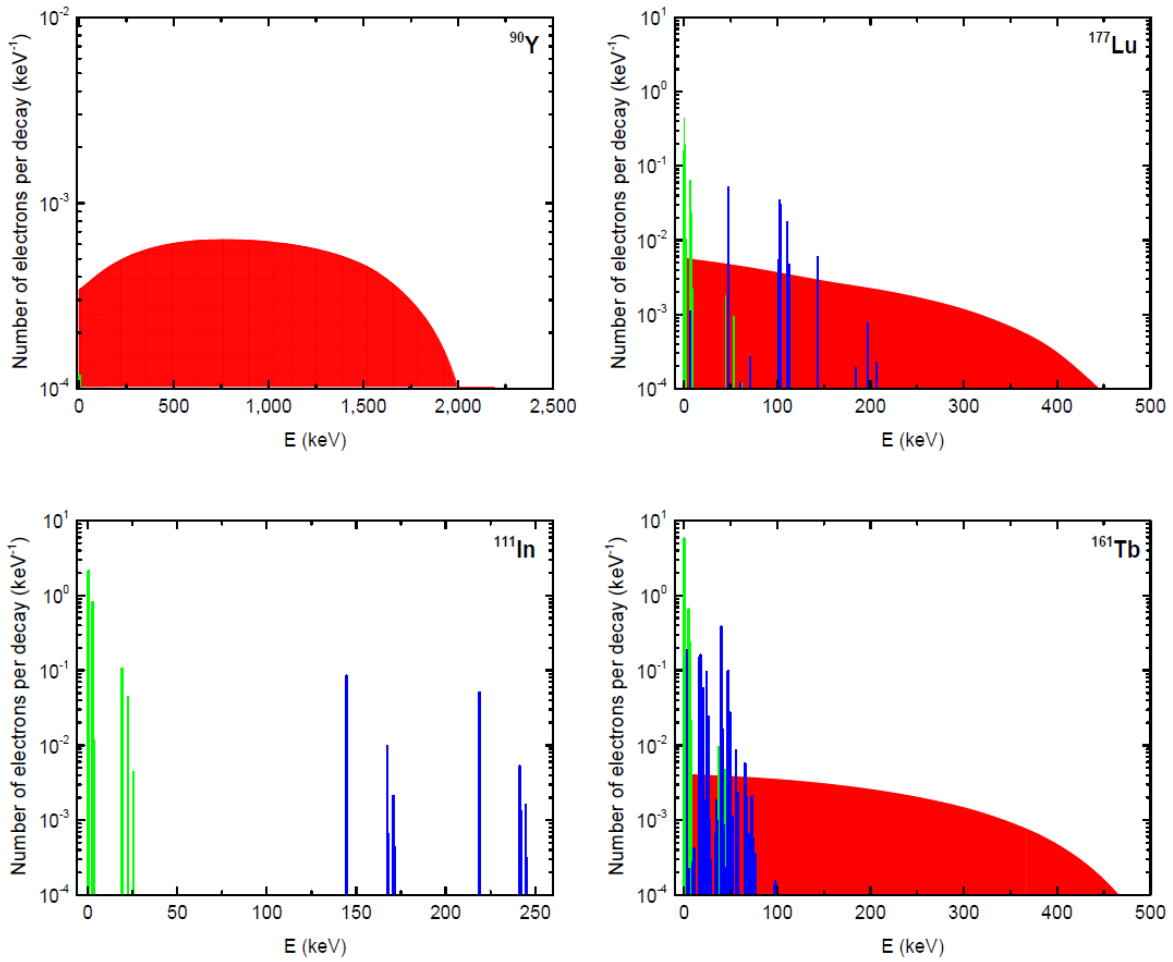


Figure-1: Electron emissions of ⁹⁰Y, ¹⁷⁷Lu, ¹¹¹In and ¹⁶¹Tb. β -spectra are in red, conversion electrons are in blue and Auger electrons in green. Conversion and Auger electrons with probability <0.0001 were neglected (21).

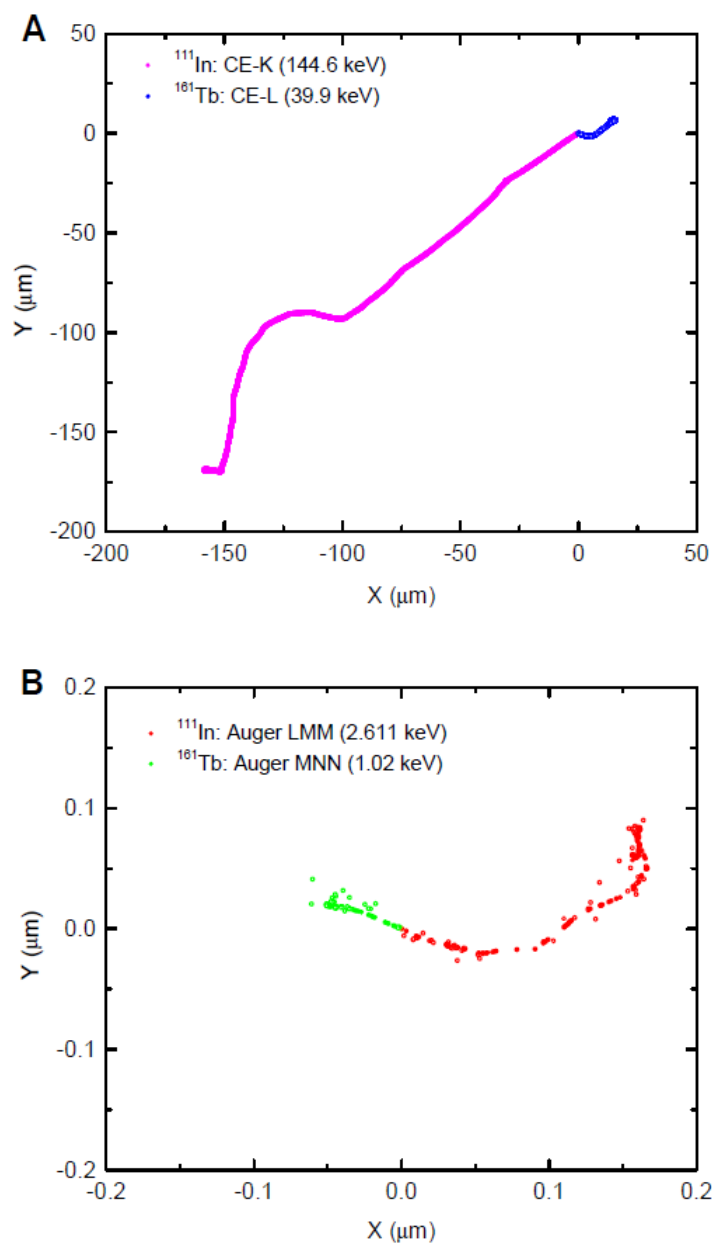


Figure-2: Tracks of representative electrons from ^{111}In and ^{161}Tb as obtained with CELLDOSE. (A) ^{111}In CE-K (144.6 keV, frequency 8.5%, magenta) and ^{161}Tb CE-L (39.9 keV, frequency 38%, blue). (B) ^{111}In Auger LMM (2.61 keV, frequency 82%, red) and ^{161}Tb Auger MNN (1.02keV, frequency 184%, green). The solid and open circles represent the ionizing interactions induced by the primary and the secondary electrons, respectively.

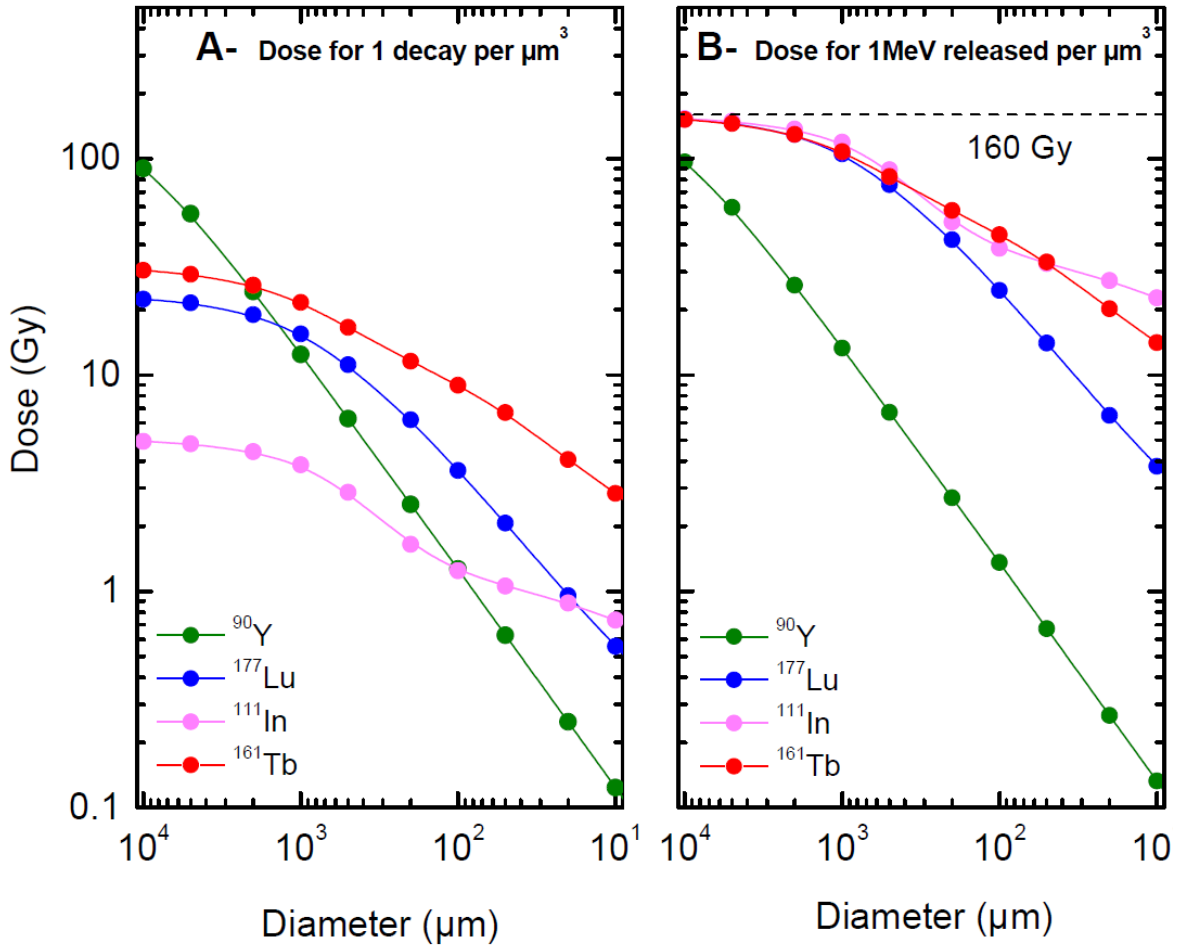


Figure-3: Electron dose from ^{90}Y (green), ^{177}Lu (blue), ^{111}In (magenta) and ^{161}Tb (red) as a function of sphere size. (A) Electron dose considering one decay per μm^3 . (B) Electron dose considering 1 MeV released per μm^3 . 160 Gy/MeV/ μm^3 corresponds to total absorption.

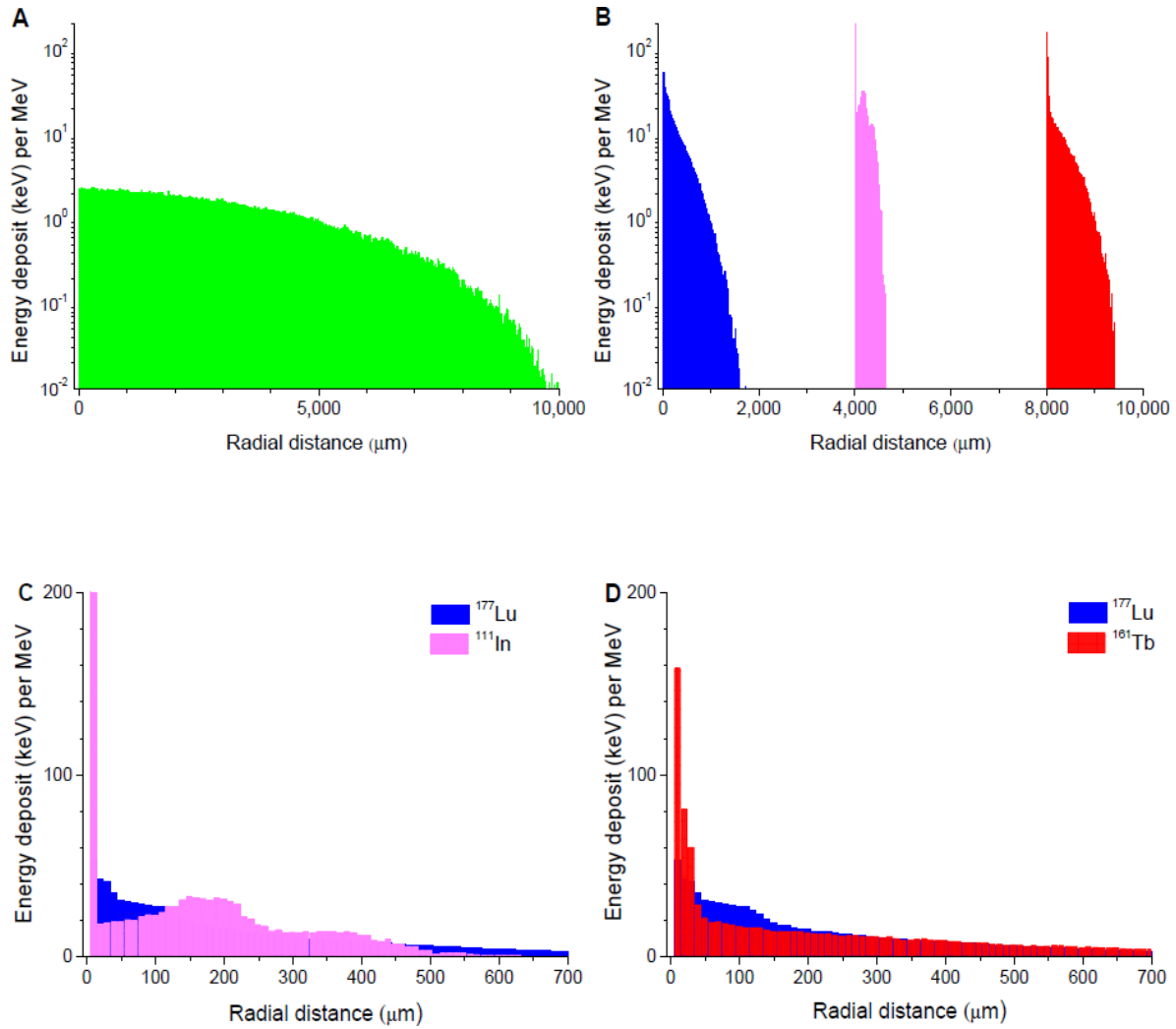


Figure-4: A and B) Energy deposit (per MeV released) within concentric shells of 10- μm thickness around a point source: ^{90}Y (green), ^{177}Lu (blue), ^{111}In (magenta) and ^{161}Tb (red). C and D) Comparisons of energy deposit in the first 700 micrometers: ^{111}In vs. ^{177}Lu (C), ^{161}Tb vs. ^{177}Lu (D). Energy deposit is in logarithmic scale in A and B and in linear scale in C and D.

Table-1: Some characteristics of the four radionuclides

Nuclide	⁹⁰ Y	¹⁷⁷ Lu	¹¹¹ In	¹⁶¹ Tb
Half-life (days)	2.671	6.647	2.805	6.906
Type of Decay (%)	β ⁻ (100 %)	β ⁻ (100 %)	EC (100%)	β ⁻ (100 %)
β particles mean energy (keV)	932.9	133.3	-	154.3
Conversion electrons (keV per decay)	0.2	13.52	27.94	39.28
CE energy range (keV)		6.2 - 206.3	144.6 – 245.4	3.3 – 98.3
Auger and Coster-Kronig electrons (keV per decay)	0.0007	1.13	6.88	8.94
Auger and Coster-Kronig electrons energy range (keV)		0.01 – 61.7	0.037 – 25.6	0.018 – 50.9
Total electron energy per decay (keV)	933.1	147.9	34.8	202.5
γ radiation useful for imaging: Energy in keV and abundance (%)	-	208.4 (11 %); 112.9 (6.4 %)	245.4 (94.1 %); 171.3 (90.6 %)	74.6 (10.2%)
Photons X and γ (total energy per decay in keV)	0.0012	35.1	405	36.35
Energy per decay in keV (photons + electrons)		183	439.8	238.9
Percentage of energy emitted as photons	~ 0	19.2 %	92.1 %	15.2 %

Table-2: Retained energy (percentage and absolute value) and contribution of the different electronic emissions

Sphere diameter (μm)	Absorbed energy (keV per decay)				Relative contribution *								
					(of different electronic emissions)			^{177}Lu			^{111}In		^{161}Tb
	^{90}Y	^{177}Lu	^{111}In	^{161}Tb	β^- (%)	CE (%)	Auger (%)	CE (%)	Auger (%)	β^- (%)	CE (%)	Auger (%)	
10,000	563	140	33.2	190	90.0	9.2	0.8	79.9	20.1	75.1	20.2	4.7	
5,000	347	135	32.2	183	89.7	9.5	0.8	79.3	20.7	74.1	21.0	4.9	
2,000	152	119	29.6	163	88.7	10.4	0.9	77.6	22.4	71.0	23.5	5.5	
1,000	77.7	96.3	25.7	135	86.9	12.0	1.1	74.2	25.8	65.5	27.9	6.6	
500	39.2	69.2	19.4	104	83.8	14.6	1.6	66.0	34.0	55.9	35.5	8.6	
200	15.8	38.6	11.2	72.3	80.1	17.1	2.8	41.8	58.2	40.1	47.7	12.2	
100	7.93	22.6	8.44	55.9	79.4	15.9	4.7	24.2	75.8	29.3	55.1	15.6	
50	3.92	13.0	7.15	41.8	77.5	14.7	7.8	13.4	86.6	21.4	58.1	20.5	
20	1.56	6.11	5.95	25.4	73.7	10.5	15.8	6.1	93.9	15.3	52.3	32.4	
10	0.77	3.62	4.96	17.7	66.1	8.2	25.7	3.5	96.5	11.7	43.4	44.9	

* For ^{90}Y , the contribution from β^- emission to energy deposit is >99%

Table-3: Comparison of electron dose deposit for the four isotopes

(also see figure-3)

Sphere diameter (μm)	Dose per decay (S-value) (Gy)				Dose for 1 decay per μm^3 (Gy)				Dose for 1 MeV released per μm^3 (Gy)			
	^{90}Y	^{177}Lu	^{111}In	^{161}Tb	^{90}Y	^{177}Lu	^{111}In	^{161}Tb	^{90}Y	^{177}Lu	^{111}In	^{161}Tb
10,000	1.72×10^{-10}	4.30×10^{-11}	1.01×10^{-11}	5.82×10^{-11}	90.1	22.5	5.31	30.5	96.5	152	153	152
5,000	8.50×10^{-10}	3.29×10^{-10}	7.88×10^{-11}	4.47×10^{-10}	55.6	21.6	5.16	29.3	59.5	145	148	146
2,000	5.80×10^{-9}	4.54×10^{-9}	1.13×10^{-9}	6.22×10^{-9}	24.3	19.0	4.74	26.0	26.0	128	136	129
1,000	2.37×10^{-8}	2.94×10^{-8}	7.86×10^{-9}	4.14×10^{-8}	12.4	15.4	4.12	21.7	13.3	104	118	108
500	9.59×10^{-8}	1.69×10^{-7}	4.75×10^{-8}	2.54×10^{-7}	6.27	11.1	3.11	16.6	6.71	74.8	89.3	82.7
200	6.03×10^{-7}	1.48×10^{-6}	4.28×10^{-7}	2.76×10^{-6}	2.53	6.18	1.79	11.6	2.70	41.8	51.5	57.6
100	2.42×10^{-6}	6.93×10^{-6}	2.58×10^{-6}	1.71×10^{-5}	1.27	3.63	1.35	8.95	1.36	24.5	38.9	44.5
50	9.58×10^{-6}	3.18×10^{-5}	1.75×10^{-5}	1.02×10^{-4}	0.63	2.08	1.14	6.67	0.67	14.1	32.9	33.3
20	5.95×10^{-5}	2.33×10^{-4}	2.28×10^{-4}	9.70×10^{-4}	0.25	0.98	0.95	4.06	0.27	6.61	27.4	20.2
10	2.37×10^{-4}	1.11×10^{-3}	1.52×10^{-3}	5.41×10^{-3}	0.12	0.58	0.79	2.83	0.13	3.92	22.8	14.1